

# SACSoN: Scalable Autonomous Data Collection for Social Navigation

Noriaki Hirose<sup>1,2</sup>, Dhruv Shah<sup>1</sup>, Ajay Sridhar<sup>1</sup> and Sergey Levine<sup>1</sup>

**Abstract**—Machine learning provides a powerful tool for building socially compliant robotic systems that go beyond simple predictive models of human behavior. By observing and understanding human interactions from past experiences, learning can enable effective social navigation behaviors directly from data. However, collecting navigation data in human-occupied environments may require teleoperation or continuous monitoring, making the process prohibitively expensive to scale. In this paper, we present a scalable data collection system for vision-based navigation, SACSoN, that can autonomously navigate around pedestrians in challenging real-world environments while encouraging rich interactions. SACSoN uses visual observations to observe and react to humans in its vicinity. It couples this visual understanding with continual learning and an autonomous collision recovery system that limits the involvement of a human operator, allowing for better dataset scaling. We use this system to collect the SACSoN dataset, the largest-of-its-kind visual navigation dataset of autonomous robots operating in human-occupied spaces, spanning over 75 hours and 4000 rich interactions with humans. Our experiments show that collecting data with a novel objective that encourages interactions, leads to significant improvements in downstream tasks such as inferring pedestrian dynamics and learning socially compliant navigation behaviors. We make videos of our autonomous data collection system and the SACSoN dataset publicly available on our project page<sup>1</sup>.

## I. INTRODUCTION

Even the simplest forms of interactions between humans, such as how to pass someone in a hallway, are governed by complex non-verbal cues, etiquette, and multi-agent coordination. In order for robots to inhabit the same environments as people, they must also be cognizant of basic social conventions and etiquette, even for seemingly simple navigational tasks. While a range of prior works have proposed approaches for modeling human behavior and human-robot interactions [1], [2], the complexity of such interactions often defies analytic modeling techniques.

Learning methods provide an appealing alternative, making it possible to acquire models or policies for navigation around humans that do not require strong assumptions about human behavior, but can instead learn how to either forecast human behavior or even directly acquire socially cognizant navigational strategies from data. Indeed, human-interactive systems have been successfully learned from data and experience in a range of other domains, such as playing games [3]–[5] and generating dialogue [6], [7]. However, the most effective modern learning techniques typically require large and representative datasets, and oftentimes the larger the dataset the more effective the resulting system can be. Therefore, in this paper we ask the question: *How can we*

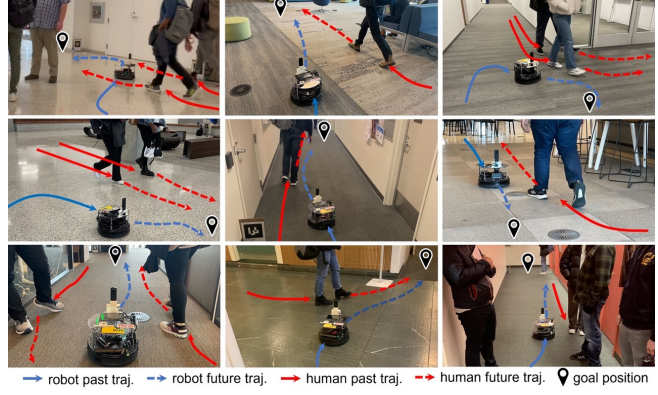


Fig. 1: SACSoN is a scalable, autonomous data collection system that encourages human-robot interactions in diverse real-world environments. We use this system to collect a dataset comprising over 75 hours of visual navigation, with over 4000 individual human-robot interactions.

*scalably collect large datasets of human-robot interaction for learning socially cognizant navigational skills?*

We are particularly concerned with making the collection process scalable, and therefore we would like to make it as automated as possible. While prior works have proposed datasets involving robotic navigation in the presence of humans, manual teleoperation makes dataset scaling costly [8], and naïve autonomous operation (e.g., driving along a pre-determined route) can lead to a relatively modest amount of human interaction [9]. Instead, we devise a learning-based system, SACSoN, that can *autonomously* collect rich interaction data with little-to-no human intervention, and can improve its data collection policy over time as the ever-growing dataset is reused to further train the collection policy.

We study how explicitly incentivizing our data collection policy to maximize human interaction leads to more useful and relevant data, and how this data collection system can be scaled with very little human effort. This is accomplished via learned vision-based navigation policies with human interaction objectives and additional mechanisms to reduce the need for manual interventions. We use the proposed system to collect the SACSoN dataset, which comprises over 75 hours of robotic navigation in 5 different office environments populated by people. To the best of our knowledge, this represents the largest such dataset of an autonomous mobile robot interacting with humans, with over 4000 individual human-robot interactions. In the process of collecting the SACSoN dataset, our robot traveled for a combined total of about 58.7 km over four months, starting in November 2022. Since our dataset includes time sequences of camera images,

<sup>1</sup>UC Berkeley, <sup>2</sup>Toyota Motor North America

[sites.google.com/view/SACSoN-review](https://sites.google.com/view/SACSoN-review)

2D LiDAR, and wheel odometry, our dataset can be useful for visual SLAM tasks including visual odometry estimation and depth estimation.

The primary contributions of this paper are two-fold: (i) an autonomous data collection system, the SACSoN system, that encourages rich interactions with human pedestrians using a novel objective, and (ii) the SACSoN dataset, a large and diverse dataset comprising over 4000 human-robot interactions of an autonomous robot operating in a densely populated office-space environment. We show that our interaction-enriched dataset can be used for a variety of downstream tasks, including human motion forecasting and learning socially compliant navigation policies for mobile robots. To the best of our knowledge, this is the largest publicly available dataset of visual navigation with social interactions publicly. Please see the project page for the dataset release, additional implementation details and videos.

## II. RELATED WORK

Social navigation has been widely studied in the past few decades [16]–[18]. Model-based approaches based on the dynamic pedestrian model have been historically applied for behavior modeling [1], [2], [19], and more recently in the context of learning forecasting models of pedestrian behavior [20], [21]. Social navigation has also been viewed through the lens of model-free data-driven learning [22]–[26], however, they tend to rely on high-fidelity simulated environments and simulated pedestrian dynamics models. Instead, we focus on learning vision-based navigation policies for social interactions directly from real-world interactions [9], [27], [28].

Data-driven approaches to vision-based navigation often use photorealistic simulators [29]–[32] or supervised data collection [33] to learn goal-reaching policies directly from raw visual observations. Instead, we focus on learning visual navigation policies from autonomously collected real-world experience, which can in principle improve continuously as more data is collected [9], [12], [34], [35]. Prior works in collecting real-world data tend to use manual teleoperation, which is expensive and scales poorly [8]–[12], [36], [37]. Instead, our work focuses on autonomous data collection of rich human-robot interactions, aiming to propose both a system for collecting such data with minimal human effort and a dataset that can be used to study policy and model learning from large autonomously-collected datasets.

While there has been prior work on autonomously collecting robot navigation data [13]–[15], [38], the task is particularly challenging due to the dynamic agents (i.e., humans) present in the environment. To autonomously learn socially-compliant behavior around humans, the training data must contain rich human-robot interactions, with humans walking close to the robot, and must include a wide perceptual and behavioral diversity — something lacking from existing autonomously collected social navigation datasets [13], [15]. The closest prior works to SACSoN are SCAND, which is teleoperated and lacks close human-robot interactions, and CoBoT, THÖR [15], [38], which are autonomous but contain

no visual observations and hence have limited utility for learning visual navigation. Table I summarizes the existing robot navigation datasets, highlighting the lack of autonomously collected datasets of social navigation behavior that can be scaled up to multiple environments and days. We propose a scalable data collection system SACSoN that can collect a large and diverse dataset of rich human interactions with an autonomous mobile robot, and can be scaled with minimal human effort to multiple environments.

## III. PRELIMINARIES

We develop our data collection system (Fig. 2) on top of a visual navigation system that can navigate to user-specified goal images using a combination of a topological graph and a learned low-level control policy. This method has been demonstrated in a variety of prior works [12], [39]–[43]. Specifically, we build our data collection system on top of ExAug [42], a topological graph-based visual navigation system that uses a model-based control policy at the low level to optimize goal-directed cost function.

The control policy predicts control velocities  $\{v_i, \omega_i\}_{i=1 \dots N_s} = \pi_{\theta_c}^c(I_t, I_g)$  from the current image  $I_t$  and subgoal image  $I_g$  and commands the linear velocity  $v_1$  and the angular velocity  $\omega_1$  to the robot to reach the position of  $I_g$ , similar to receding horizon control. Here,  $N_s$  is the control horizon. This control policy is paired with a topological memory that contains images as nodes and temporal distance between them as the edges. The ExAug control policy  $\pi_{\theta_c}$  is trained using supervised learning to minimize the objective

$$J_{\text{exaug}}(\theta_c) := J_{\text{pose}}(\theta_c) + w_c J_{\text{col}}(\theta_c) + w_r J_{\text{reg}}(\theta_c), \quad (1)$$

where  $J_{\text{pose}}$  corresponds to the prediction error in the relative pose estimates,  $J_{\text{col}}$  penalizes collisions, and  $J_{\text{reg}}$  is a regularization term for predicted velocities. Please refer to the original paper for implementation details of this system [42]. SACSoN system builds upon ExAug along two key axes: by encouraging interactions with human pedestrians using a novel cost function (Sec. IV), and automating the deployment of the navigation system for scalable data collection without human interventions (Sec. V).

## IV. ENCOURAGING INTERACTIONS WITH SACSON

To encourage human-directed interactions, we modify our visual navigation backbone by proposing a novel objective that encourages the robot to drive closer to humans in the environment, causing humans to interact with the robot. We formulate this objective  $J_{\text{int}}$  as the *interaction loss*, that expresses the distance of the robot to the nearest pedestrian in the scene, and encourage the robot to minimize this objective during the training of our data collection policy. The modified training objective thus becomes

$$\min_{\theta} J(\theta) := J_{\text{exaug}}(\theta) + w_i J_{\text{int}}(\theta), \quad (2)$$

where  $w_i$  is a scaling factor, and  $\theta$  represents the learnable parameters of our control policy. Here, our control policy predicts velocity commands  $\{v_i, \omega_i\}$  and operates on the

Dataset	Human	Policy	Duration [hour]	Distance [km]	Sensors
KITTI odometry [10]	✗	teleop	0.7	22.2	stereo RGB, 3D LiDAR, GPS
NCLT [11]	✗	teleop	34.9	147.4	RGB, 3D LiDAR, odom, GPS, IMU
GO Stanford [12]	✗	teleop	10.3	16.7	spherical RGB, odom
FLOBOT [13]	✗	autonomous	0.46	0.2	RGBD, stereo RGB, 3D and 2D LiDAR, odom, IMU.
RECON [14]	✗	autonomous	25.0	81.0	stereo fisheye RGBD, thermal, 2D LiDAR, GPS, IMU
JRDB [8]	✓	teleop	1.1	2.3	stereo RGBD, 3D and 2D LiDAR, IMU
SCAND [9]	✓	teleop	8.7	40.0	RGBD, 3D LiDAR, odom
THÖR [15]	✓	scripted	1.0	1.0	3D LiDAR, motion capture, eye-tracking glasses
SACSoN (Ours)	✓	autonomous	75.0	58.7	spherical RGBD, fisheye RGB, 2D LiDAR, odom, bumper

TABLE I: Survey of public datasets for learning vision-based navigation policies in real-world environments around humans. SACSoN is the largest publicly available visual navigation dataset of an autonomous policy interacting with humans in real-world environments.

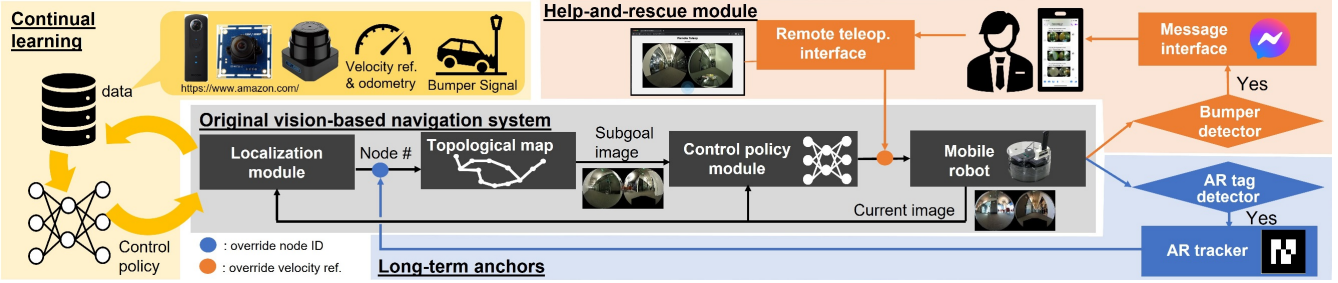


Fig. 2: SACSoN System overview. We design our autonomous data collection platform around a vision-based navigation system (gray) that uses a topological graph and a learned control policy. Our proposed system has three key components: a help-and-rescue module for collision recovery (orange), long-term anchors for localization (blue), and continual learning (yellow).

robot's past observations  $I_{t:t-N_p}$ , and the goal observation  $I_g$ , defined as follows:

$$\{v_i, \omega_i\}_{i=1\dots N_s} = \pi_\theta(I_{t:t-N_p}, I_g) \quad (3)$$

Concatenating the past image frames gives the robot additional context that can be useful to avoid obstacles, detect pedestrians in the environment and reduce partial observability [44].

During training, we use YOLO [45], [46] and DeepSORT [47] to detect and track pedestrians in the recorded images (processed into a panorama) from the recorded observations of the robot [48], and project these detections in 3D using the depth and scale estimates [49] obtained from the ExAug perception module, as shown in Fig. 3. We use these position estimates for each of the 4000+ humans encountered in the training dataset to define the interaction loss. This loss is designed to minimize the distance between human and robot trajectories as follows

$$J_{\text{int}}(\theta) = \min_i \{|r_i - h_i|\}, \quad (4)$$

where  $\mathcal{R} = \{r_1, r_2, \dots, r_{N_s}\}$  and  $\mathcal{H} = \{h_1, h_2, \dots, h_{N_s}\}$  are the estimated trajectories of the robot and human, respectively.  $r_i$  is robot's position estimate at time  $i$  on top-down 2D plane, which is calculated by integrating velocity commands  $\{v_i, \omega_i\}_{i=1\dots N_s}$ .  $h_i$  is the *nearest* non-stationary pedestrian's position in the robot's local frame at time  $i$ . Intuitively, this objective denotes the closest distance between the robot and pedestrian during their interaction, and optimizing Eqn. 2 would result in the best parameter  $\theta$  that minimizes

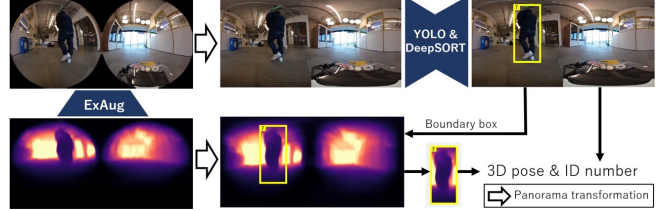


Fig. 3: Pedestrian detection and tracking. We use a combination of YOLO and DeepSORT to detect and track pedestrians from visual observations, and estimate their relative position using the scaled depth estimates from ExAug's perception module.

this closest distance of interaction.  $J_{\text{int}}$  may be alternatively defined as the mean of the set  $\{|r_i - h_i|\}$ , but empirically, we found the min formulation of Eqn. 4 to better capture the desired interaction behavior.

## V. AUTONOMOUS DATA COLLECTION SYSTEM

We design a scalable data collection system that is largely autonomous and can operate in large, indoor environments without any high-fidelity indoor positioning system (like Vicon). Our proposed system (see Fig. 2) builds on top of the existing ExAug visual navigation system using three key components: (a) help-and-rescue module for collision recovery, (b) long-term anchors for coarse localization in the environment, and (c) continual learning for improving performance over the course of deployment.

**Help-and-rescue module:** To make the data collection process as seamless and autonomous as possible, we designed

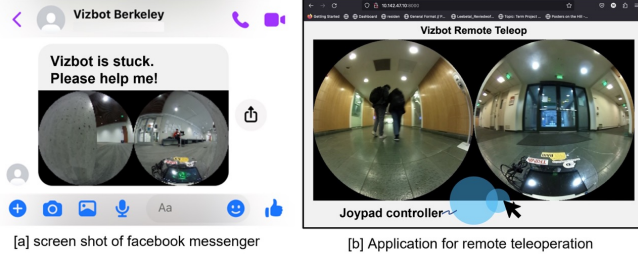


Fig. 4: **Help-and-rescue module.** The robot messages the operator for assistance when stuck (left), and can be rescued remotely over the internet using our web interface (right).

a pipeline for autonomous recovery from collisions and seeking remote help in case of irrecoverable collisions. When a collision is detected by the robot’s collision detector sensor, an automatic backup maneuver is executed. This maneuver drives the robot away from the obstacle for a short distance along the normal vector corresponding to the point of contact. This allows the robot to automatically recover from 70% of the simple collisions where the robot accidentally runs into challenging obstacles (e.g., that may be shorter than the camera height, made of glass etc.). Complete autonomy, however, may not be possible to achieve. The robot may drive itself into a convex hull of multiple obstacles, leading to repeated collisions, or get its wheels stuck (e.g., on an air vent) and be unable to rescue itself.

We built a messaging and remote teleoperation interface where the robot sends a signal to a remote operator for help over the internet, and the remote operator can take control of the robot over the internet to drive the robot out of the tricky situation (Fig. 4). This simple interface also enables fleet operations, where a single operator can monitor and assist a large fleet of robots to enable data collection at scale. This module allows the robot to recover from 95% of the more difficult situations, with only a handful cases requiring a physical intervention.

**Long-term anchors:** While topological memory with image nodes has been used in a variety of navigation applications, it struggles to scale for large, repetitive environments due to challenges in perceptual aliasing (e.g. all office hallways, desks, and doors look alike). This can create ambiguities in the robot’s current position on the graph, jeopardizing the capabilities of the robot to collect reliable “ground-truth” positions for annotating the collected dataset.

To overcome this limitation, we augment the topological navigation framework of ExAug with a small numbers of anchor nodes in the real-world environment that are tagged with Alvar AR tags [50]. Before deployment, we place AR tags throughout the environment at approximately 10 meters apart, which corresponds to over 100 time steps: a large distance for a small indoor robot. Since these tags are located at fixed anchor locations, we can use their coarse positions to the corresponding nodes of our topological graph. When the robot observes one of these anchors, we override the underlying localization estimate of the robot with the node corresponding to the anchor to, reducing perceptual aliasing in long-term localization. Please see the supplemental mate-

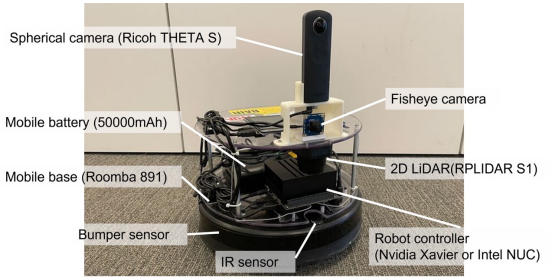


Fig. 5: **Data collection platform.** We collect spherical and fisheye RGB images, 2D LiDAR, global odometry (using long-term visual anchors), and bumper signals using our robotic system.

rial on our project page for more information on long-term localization.

**Continual learning:** As the data collection system is deployed, it may encounter novel challenges—such as varying environmental lighting throughout the day, new obstacles in the environment etc.—and it must adapt the learned data collection behavior to these changes. To achieve this, our system adopts a continual learning approach, where training data at the end of each day of deployment is used to *fine-tune* the data collection policy to incorporate new experience. We also use data collected across multiple days, and times of day, to augment the fine-tuning data by chaining diverse trajectory segments between the same subgoals [51]. This allows us to effectively incorporate experience in the deployment environment over multiple days, while also improving robustness to variations across different days and times of day. Please see our supplemental materials for more information on trajectory chaining.

## VI. THE SACSON DATASET

We use the system discussed in the preceding section to autonomously collect over 75 hours of robot navigation data in 5 diverse human-occupied environments, capturing over 4000 rich interactions with humans. This section describes the robotic system used for data collection environment setup, as well as key characteristics of the dataset.

### A. Robot and Environment Setup

Figure 5 shows an overview of our data collection platform, built on top of an iRobot Roomba base [49], [52]. The robot is equipped with two visual sensors (a spherical camera, and a 170° wide-angle RGB camera), and a 2D LiDAR. We use two identical data collection robots with identical sensors, equipped with different onboard computers: an NVIDIA Jetson Xavier AGX, and an Intel i5 NUC, with all computation run onboard without a dedicated GPU. Our system commands angular and linear velocity commands to the base, and has access to the bumper collision sensor for triggering our help-and-rescue module.

During deployment, we instrument the environment with  $N_{AR}$  AR tags to coarsely define the robot’s route for data collection (approximately 10 m apart), and collect an example trajectory by teleoperation. This example trajectory is subsampled at a fixed frame rate of 0.5 fps to generate a topological graph of the environment. Additionally, we associate

each AR tag with neighboring image nodes by collecting their ID and relative pose estimates in the robot’s local frame. Starting with a *base* control policy that does not encourage human interactions, SACSoN system autonomously collects data that is used to train a new control policy that can interact with humans (Section IV) and can improve with increasing environmental experience (Section V). Please see our supplemental materials for further details.

**Implementation details:** We empirically set the interaction weight  $w_i = 1.5$ , after analyzing closed-loop navigation performance. Following ExAug [42], we set the control horizon  $N_s = 8$  and the past observations  $N_p = 5$  (see Eqn. 3). For pedestrian detection and tracking, we use the spherical camera on the robot to allow detection and interactions with pedestrians behind it. For the trajectory chaining procedure described in Section V, we merge multiple trajectories across several days from an environment to enhance robustness to visual distractors. We use a batch size of 80, with the training pair (past observations and subgoal images) sampled from the same trajectory for one half of the batch, and the pair coming from different trajectories in the other half of the batch. All other hyperparameters are replicated from ExAug [42].

### B. Dataset Characteristics

We collected the SACSoN dataset over the course of 24 days in 5 diverse environments, spread across 3 university buildings. The dataset spans 75 hours and 58 kilometers of autonomous robot navigation trajectories, containing over 4000 interactions with humans. The dataset includes visual observations (spherical and fisheye), 2D LiDAR scans, global position estimates (using the long-term anchors), velocity information, and collision signals from the bumper. Figure 6 shows example images of rich human-robot interactions captured in our dataset. We have released this dataset publicly on our project page.

**Quantifying human interactions:** To evaluate the efficacy of the proposed interaction objective  $J_{\text{int}}$  (Section IV), our dataset contains two equal subsets: the *interaction-enriched dataset* corresponding to data collected by the collection policy with interaction objective ( $w_i = 1.5$ ), and the *naive dataset* collected without ( $w_i = 0$ ). To understand the effect of the proposed interaction loss on the quality of the data collected, we conduct controlled experiments with 5 human participants tasked with interacting with the data collection system running two different collection policies: one that encourages interactions and another that does not.

While quantifying the amount of human interaction is a challenging problem by itself [53], we propose three metrics that coarsely capture these interactions: (i) the mean distance of the robot to an observed pedestrian, (ii) bounding box area (in sq. pixels) of the observed pedestrian, as detected by an object detector [45], and (iii) the offset (in pixels) of the observed pedestrian from the center of the robot’s frame (e.g., this would correspond to the visual servoing error for a follower robot [54]). Table II shows the results of this evaluation on the two subsets of our dataset. We observe that the interaction-enriched dataset results in collection

Dataset	Distance [m] ↓	Area [px <sup>2</sup> ] ↑	Offset [px] ↓
no $J_{\text{int}}$	2.67	$0.99 \times 10^4$	128.51
Ours (Eqn. 4)	<b>2.43</b>	<b><math>1.40 \times 10^4</math></b>	<b>98.55</b>

TABLE II: **Evaluation of the interaction objective.** A policy trained on the interaction-enriched dataset (with  $J_{\text{int}}$ ) drives closer to the pedestrians, and captures more prominent interactions.

policies that drive closer to the pedestrians, and captures more prominent interactions.

### VII. EVALUATING LEARNED BEHAVIORS WITH SACSON

We design our experiments to evaluate the proposed interaction-enriched dataset, as well as the autonomous data collection system, towards the following questions:

- Q1.** Does the proposed interaction objective lead to learning better predictive models of pedestrian behavior?
- Q2.** Do social navigation policies trained with the interaction-enriched dataset lead to more engagement, as compared to the naïve dataset?
- Q3.** How does the performance of the data collection system evolve with increasing experience?

### A. Modeling Pedestrian Dynamics

Modeling and forecasting pedestrian behavior is an important milestone towards robotic systems that can interact with humans, and has been studied in a wide variety of applications [8], [55], [56]. We assess the efficacy of SACSoN dataset, collected with our proposed interaction objective, in training a conditional predictive model of human motion that captures the effects of the robot’s plans on the human’s future motion in challenging, indoor environments.

To evaluate this, we use two subsets of the dataset collected with and without the proposed interaction objective, as described in Section VI-B. We train a predictive model  $f_{\theta_p}$  of a pedestrian’s future trajectory, conditioned on their past trajectory, as well as the robot’s past and future plans, i.e.  $f_{\theta_p}(\hat{h}_{t:t+\beta}|h_{t-\alpha:t-1}, r_{t-\alpha:t+\beta})$ , where  $r_i$  denotes past and future robot positions,  $h_i$  denotes past pedestrian positions, and  $\hat{h}_i$  denotes the estimated future positions of the pedestrian. All positions are represented in a 2D plane with origin at  $r_t$ . The predictive model is conditioned on  $\alpha = 7$  past observations, and predicts  $\beta = 8$  future observations at each time step. For simplicity, we only consider scenes involving with a single pedestrian; for scenes with multiple pedestrians, we only consider nearest non-stationary pedestrian for training, since they are most likely to interact with the robot. We train  $f_{\theta_p}$  on each trajectory in the training data by minimizing the MSE loss using supervised learning. While more sophisticated algorithms for learning pedestrian forecasting models may be employed [20], [21], we emphasize that our objective is to evaluate the effectiveness of the interaction-enriched dataset for training a *given* predictive model, and not to train the best predictive model.

We report the mean squared error, to capture how close each predicted point is to the true future positions, and the cosine similarity score, that measures the alignment between



Fig. 6: **Example scenes from the SACSoN Dataset.** We collected our dataset in 5 different environments, spanning over 75 hours of data collection and 4000 rich human interactions, containing raw visual observations (cropped spherical images shown here).

Dataset	MSE $\downarrow$	Cosine $\uparrow$
no $J_{\text{int}}$	0.0278	0.615
Ours (Eqn. 4)	<b>0.0231</b>	<b>0.689</b>

TABLE III: **Training a Pedestrian Dynamics Model.** Training on the interaction-enriched dataset leads to better predicted trajectories.

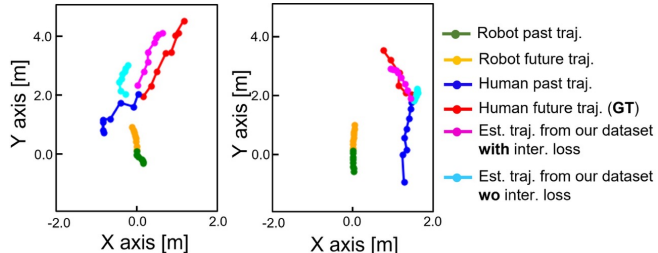


Fig. 7: **Examples of using the learned human dynamics model to predict future human positions**, conditioned on past human positions (blue), past robot positions (green), and future robot plans (yellow). Training with the interaction-enriched dataset (magenta) leads to better predictions than the naïve dataset (blue).

the vectors corresponding to the predicted and true positions (a scale-invariant metric that better captures directional information [44]). Table III shows the evaluation results of the predictive model trained on the two subsets of SACSoN dataset. We find that a predictive model trained with the interaction-enriched dataset leads to better predictions, both in terms of the direction and scale, suggesting that the proposed objective indeed allows better prediction of future human behavior. Fig. 7 illustrates the predictive model in action for two example interactions.

### B. Learning Socially Compliant Navigation

One of the simplest forms of socially compliant behavior is to avoid intruding someone’s personal space. In this section, we consider a simple way to use the collected dataset to facilitate learning social navigation behavior of this form. We modify the policy learning method that we employed to collect our dataset (Section IV), but with the weight on the human interaction term  $w_i$  negated to penalize proximity to humans. Optimizing this new objective would discourage the robot from getting too close to a pedestrian’s personal space and interacting with them.

Towards answering **Q2**, we train two different social navigation policies corresponding to the two subsets of the

Dataset	$J(\theta) \downarrow$	$J_{\text{int}}(\theta) \uparrow$	$J_{\text{pose}}(\theta) \downarrow$	$J_{\text{geo}}(\theta) \downarrow$
no $J_{\text{int}}$	-1.153	1.014	0.0886	$1.717 \times 10^{-4}$
Ours (Eqn. 4)	<b>-1.236</b>	<b>1.063</b>	<b>0.0866</b>	<b><math>1.318 \times 10^{-4}</math></b>

TABLE IV: **Evaluating Social Navigation.** In offline evaluations, we find a policy trained with the interaction-enriched dataset results in better objective values for social navigation.

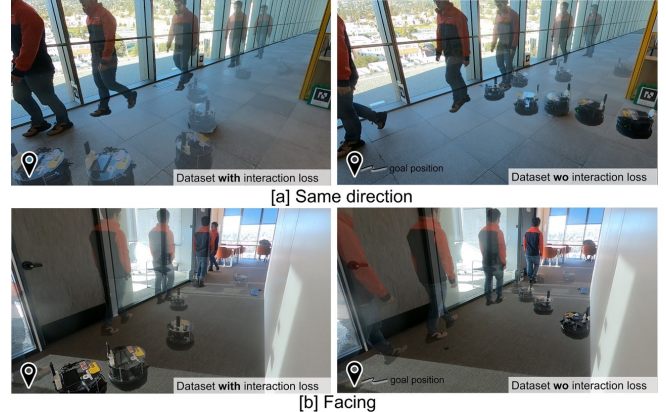


Fig. 8: **Qualitative Examples of Learned Behavior.** A social navigation policy trained on the interaction-enriched subset of SACSoN (left) leads to better handling of human pedestrians while successfully reaching the goal, without intruding in their personal space. Training on the naïve dataset results in a conservative policy (right) that avoids humans and loses track of the goal.

training data. Table IV shows the values of the optimization objectives, as evaluated “offline” on a held-out navigation trajectory around humans: a control policy trained on the interaction-enriched dataset leads to an overall lower objective  $J$ , as well as *lower* interaction (i.e., higher  $J_{\text{int}}$ ).

Deploying these learned policies on the robotic system described in Section VI-A, we qualitatively observe the robot’s behavior to be significantly more “compliant” when trained with the interaction-enriched dataset (see Fig. 8). While the policy trained with the naïve dataset is good at avoiding collisions with the pedestrian, it often strays too far in order to avoid collision (right), and loses localization; the policy trained with the interaction-enriched dataset, however, has learned socially compliant behavior of walking along the human albeit at a farther distance and succeeds in reaching the goal while keeping the pedestrian’s personal space (left).

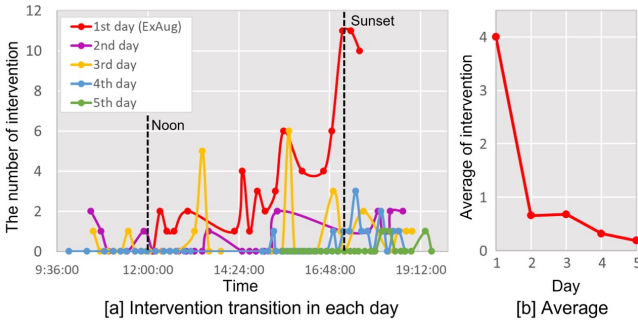


Fig. 9: **Self-Improvement with Continual Learning.** SACSoN can improve with increasing experience, a 95.5% reduction in interventions over the course of 5 days (right). While the performance varies across times of day due to variability in appearances (left, red), continual learning enables our system to eventually learn consistent collision-free behavior across the day (green).

### C. Continual Learning with the SACSoN System

Finally, we evaluate the ability of the autonomous data collection system (Section V) to improve with increasing amounts of experience after deployment. We deploy our system in a challenging office-like environment for up to 8 hours per day, for 5 days, to autonomous collect data. Over the course of this deployment, the environment would undergo significant changes in visual appearance (e.g., between the lighting through glass walls in the morning and after sunset), as well as in the structure of the environment (e.g., new desks and phone rooms were added to the environment on some of the days), and any practical real-world deployed system must adapt to these changes over time.

To simplify the evaluation, we trained a navigation policy with  $w_i = 0$  to isolate the effects of the data collection system without any human interactions. During deployment, SACSoN system operates autonomously, with occasional remote assistance, to collect data through the environment. At the end of a collection day, this data is used to *fine-tune* the collection policy to incorporate the new experience (as described in Sec. V).

Figure 9(a) shows the average number of remote interventions requested by the data collection during the different times of day. We notice that at the start, the variability in environmental lighting is significant and the initialized model (red) performs significantly worse as the day progresses. However, SACSoN system is able to quickly incorporate this new experience and improve its performance in subsequent data collection days, requiring fewer interventions each time. Over the course of multiple days (b), our system learns near-perfect autonomous navigation in the challenging indoor environment with dynamic obstacles, requesting an average of 0.18 interventions per a 10 minute trajectory, representing a 95.5% improvement over the day 1 baseline.

## VIII. DISCUSSION

In this paper, we proposed SACSoN, a scalable data collection system with a novel interaction enriching objective

that encourages robots to autonomously navigate in human-occupied spaces. Our system is very modular, can be built around an existing vision-based navigation system, and has three key components: (i) a help-and-rescue module for collision recovery and seeking remote assistance, (ii) a long-term localization module that uses AR markers placed around the environment for coarse guidance, and (iii) a continual learning framework that allows the system’s performance to improve with increasing experience. We used this data collection system to collect the SACSoN dataset: the largest-of-its-kind publicly available dataset of visual navigation around humans, spanning over 75 hours of data collected in 5 different environments and comprising over 4000 rich human-robot interactions. Our experiments show that collecting a large dataset with an interaction enriching objective can lead to improvements in downstream tasks, such as improved pedestrian behavior modeling and learning socially compliant navigation behavior in real-world environments.

Our instantiation of the autonomous data collection principle does have some limitations. Most prominently, our autonomous robot is restricted to operate at slow speeds (capped at 0.4 m/s) to limit damage due to policy errors in safety-critical environments with humans; however, this inherently limits the quality of interactions observed by the robot. Humans walking at a casual pace are much faster than the robot, and tend to not interact closely with the robot, for instance, to give right-of-way, or open the door etc. The trade-off between capturing complex social interactions, and staying safe around humans, needs to be studied carefully to result in more interactive systems that demonstrate complex, cooperative behaviors. Additionally, our current system only learns simple social interactions such as avoiding personal a pedestrian’s space; learning richer social interactions will need better objectives incorporated more tightly in the data collection and deployment policies.

## ACKNOWLEDGMENTS

This research was supported by Berkeley DeepDrive at the University of California, Berkeley, and Toyota Motor North America. Additionally, partial support for this research was provided by ARL DCIST CRA W911NF-17-2-0181. The authors would like to express their gratitude to Marwa Abdulhai, Qiyang Li, Manan Tomar, and Mitsuhiro Nakamoto for their valuable assistance in evaluating the SACSoN.

## REFERENCES

- [1] D. Helbing *et al.*, “Social force model for pedestrian dynamics,” *Physical review E*, vol. 51, no. 5, p. 4282, 1995. 1, 2
- [2] G. Ferrer *et al.*, “Robot companion: A social-force based approach with human awareness-navigation in crowded environments,” in *2013 IEEE/RSJ International Conference on Intelligent Robots and Systems*. IEEE, 2013, pp. 1688–1694. 1, 2
- [3] D. Silver *et al.*, “Mastering chess and shogi by self-play with a general reinforcement learning algorithm,” *arXiv preprint arXiv:1712.01815*, 2017. 1
- [4] O. Vinyals *et al.*, “Starcraft ii: A new challenge for reinforcement learning,” *arXiv preprint arXiv:1708.04782*, 2017. 1
- [5] J. Kramár *et al.*, “Negotiation and honesty in artificial intelligence methods for the board game of diplomacy,” *Nature Communications*, vol. 13, no. 1, p. 7214, 2022. 1

[6] P. Mirowski *et al.*, “Co-writing screenplays and theatre scripts with language models: An evaluation by industry professionals,” *arXiv preprint arXiv:2209.14958*, 2022. 1

[7] N. Stiennon *et al.*, “Learning to summarize with human feedback,” *Advances in Neural Information Processing Systems*, vol. 33, pp. 3008–3021, 2020. 1

[8] R. Martin-Martin *et al.*, “Jrdb: A dataset and benchmark of egocentric robot visual perception of humans in built environments,” *IEEE transactions on pattern analysis and machine intelligence*, 2021. 1, 2, 3, 5

[9] H. Karnan *et al.*, “Socially compliant navigation dataset (scand): A large-scale dataset of demonstrations for social navigation,” *IEEE Robotics and Automation Letters*, 2022. 1, 2, 3

[10] A. Geiger *et al.*, “Are we ready for autonomous driving? the kitti vision benchmark suite,” in *Conference on Computer Vision and Pattern Recognition (CVPR)*, 2012. 2, 3

[11] N. Carlevaris-Bianco *et al.*, “University of michigan north campus long-term vision and lidar dataset,” *The International Journal of Robotics Research*, vol. 35, no. 9, pp. 1023–1035, 2016. 2, 3

[12] N. Hirose *et al.*, “Deep visual mpc-policy learning for navigation,” *IEEE Robotics and Automation Letters*, 2019. 2, 3

[13] Z. Yan *et al.*, “Robot perception of static and dynamic objects with an autonomous floor scrubber,” *Intelligent Service Robotics*, 2020. 2, 3

[14] D. Shah *et al.*, “Rapid exploration for open-world navigation with latent goal models,” in *Annual Conference on Robot Learning (CoRL)*, 2021. 2, 3

[15] A. Rudenko *et al.*, “Thör: Human-robot navigation data collection and accurate motion trajectories dataset,” *IEEE Robotics and Automation Letters*, vol. 5, no. 2, pp. 676–682, 2020. 2, 3

[16] C. Mavrogiannis *et al.*, “Core challenges of social robot navigation: A survey,” *arXiv preprint arXiv:2103.05668*, 2021. 2

[17] E. A. Sisbot *et al.*, “A human aware mobile robot motion planner,” *IEEE Transactions on Robotics*, vol. 23, no. 5, pp. 874–883, 2007. 2

[18] J. Mumm and B. Mutlu, “Human-robot proxemics: physical and psychological distancing in human-robot interaction,” in *international conference on Human-robot interaction*, 2011. 2

[19] D. Mehta *et al.*, “Autonomous navigation in dynamic social environments using multi-policy decision making,” in *2016 IEEE/RSJ International Conference on Intelligent Robots and Systems (IROS)*. IEEE, 2016, pp. 1190–1197. 2

[20] A. Alahi *et al.*, “Social lstm: Human trajectory prediction in crowded spaces,” in *Proceedings of the IEEE conference on computer vision and pattern recognition*, 2016, pp. 961–971. 2, 5

[21] A. Sadeghian *et al.*, “Sophie: An attentive gan for predicting paths compliant to social and physical constraints,” in *conference on computer vision and pattern recognition*, 2019. 2, 5

[22] Y. F. Chen *et al.*, “Socially aware motion planning with deep reinforcement learning,” in *2017 IEEE/RSJ International Conference on Intelligent Robots and Systems (IROS)*. IEEE, 2017, pp. 1343–1350. 2

[23] ———, “Decentralized non-communicating multiagent collision avoidance with deep reinforcement learning,” in *2017 IEEE international conference on robotics and automation (ICRA)*. IEEE, 2017, pp. 285–292. 2

[24] M. Everett *et al.*, “Motion planning among dynamic, decision-making agents with deep reinforcement learning,” in *International Conference on Intelligent Robots and Systems (IROS)*. IEEE, 2018. 2

[25] C. Chen *et al.*, “Crowd-robot interaction: Crowd-aware robot navigation with attention-based deep reinforcement learning,” in *international conference on robotics and automation (ICRA)*. IEEE, 2019. 2

[26] Y.-J. Mun *et al.*, “Occlusion-aware crowd navigation using people as sensors,” *arXiv preprint arXiv:2210.00552*, 2022. 2

[27] A. Pokle *et al.*, “Deep local trajectory replanning and control for robot navigation,” in *2019 international conference on robotics and automation (ICRA)*. IEEE, 2019, pp. 5815–5822. 2

[28] M. Luber *et al.*, “Socially-aware robot navigation: A learning approach,” in *2012 IEEE/RSJ International Conference on Intelligent Robots and Systems*. IEEE, 2012, pp. 902–907. 2

[29] Manolis Savva\*, Abhishek Kadian\*, Oleksandr Maksymets\*, Y. Zhao, E. Wijmans, B. Jain, J. Straub, J. Liu, V. Koltun, J. Malik, D. Parikh, and D. Batra, “Habitat: A Platform for Embodied AI Research,” in *International Conference on Computer Vision (ICCV)*, 2019. 2

[30] F. Xia *et al.*, “Gibson env: Real-world perception for embodied agents,” in *Proceedings of the IEEE conference on computer vision and pattern recognition*, 2018. 2

[31] M. Savva *et al.*, “Minos: Multimodal indoor simulator for navigation in complex environments,” *arXiv preprint arXiv:1712.03931*, 2017. 2

[32] E. Kolve *et al.*, “Ai2-thor: An interactive 3d environment for visual ai,” *arXiv preprint arXiv:1712.05474*, 2017. 2

[33] A. Francis *et al.*, “Long-range indoor navigation with prm-rl,” *IEEE Transactions on Robotics*, vol. 36, no. 4, pp. 1115–1134, 2020. 2

[34] D. Shah *et al.*, “Ving: Learning open-world navigation with visual goals,” in *2021 IEEE International Conference on Robotics and Automation (ICRA)*. IEEE, 2021, pp. 13 215–13 222. 2

[35] S. Levine and D. Shah, “Learning robotic navigation from experience: principles, methods and recent results,” *Philosophical Transactions of the Royal Society B*, 2023. 2

[36] N. Hirose *et al.*, “Gonet: A semi-supervised deep learning approach for traversability estimation,” in *2018 IEEE/RSJ International Conference on Intelligent Robots and Systems (IROS)*. IEEE, 2018, pp. 3044–3051. 2

[37] ———, “Vunet: Dynamic scene view synthesis for traversability estimation using an rgb camera,” *IEEE Robotics and Automation Letters*, vol. 4, no. 2, pp. 2062–2069, 2019. 2

[38] J. Biswas and M. M. Veloso, “Localization and navigation of the cobots over long-term deployments,” *The International Journal of Robotics Research*, vol. 32, no. 14, pp. 1679–1694, 2013. 2

[39] N. Savinov *et al.*, “Semi-parametric topological memory for navigation,” in *International Conference on Learning Representations*, 2018. 2

[40] X. Meng *et al.*, “Scaling local control to large-scale topological navigation,” in *2020 IEEE International Conference on Robotics and Automation (ICRA)*. IEEE, 2020, pp. 672–678. 2

[41] D. Shah *et al.*, “Viking: Vision-based kilometer-scale navigation with geographic hints,” *arXiv preprint arXiv:2202.11271*, 2022. 2

[42] N. Hirose *et al.*, “ExAug: Robot-Conditioned Navigation Policies via Geometric Experience Augmentation,” in *International Conference on Robotics and Automation (ICRA)*, 2023. [Online]. Available: <https://arxiv.org/abs/2210.07450> 2, 5

[43] N. Kim *et al.*, “Topological Semantic Graph Memory for Image Goal Navigation,” in *CoRL*, 2022. 2

[44] D. Shah *et al.*, “GNM: A General Navigation Model to Drive Any Robot,” in *International Conference on Robotics and Automation (ICRA)*, 2023. [Online]. Available: <https://arxiv.org/abs/2210.03370> 3, 6

[45] J. Redmon *et al.*, “You only look once: Unified, real-time object detection,” in *Proceedings of the IEEE conference on computer vision and pattern recognition*, 2016, pp. 779–788. 3, 5

[46] ———, “Object detection by yolov5,” <https://github.com/ultralytics/yolov5>. 3

[47] N. Wojke *et al.*, “Simple online and realtime tracking with a deep association metric,” in *2017 IEEE international conference on image processing (ICIP)*. IEEE, 2017, pp. 3645–3649. 3

[48] ———, “Pedestrian detection and tracking by yolov5 and deepsort,” [https://github.com/HowieMa/DeepSORT\\_YOLOv5\\_Pytorch](https://github.com/HowieMa/DeepSORT_YOLOv5_Pytorch). 3

[49] T. Niwa *et al.*, “Spatio-temporal graph localization networks for image-based navigation,” in *International Conference on Intelligent Robots and Systems (IROS)*. IEEE, 2022. 3, 4

[50] “Ros wrapper for alvar, an open source ar tag tracking library,” [http://wiki.ros.org/ar\\_track\\_alvar](http://wiki.ros.org/ar_track_alvar). 4, 9

[51] Y. Chebotar *et al.*, “Actionable models: Unsupervised offline reinforcement learning of robotic skills,” *arXiv preprint arXiv:2104.07749*, 2021. 4

[52] ———, “Ros driver irobot roomba,” <https://github.com/AutonomyLab/create-robot>. 4

[53] J. Wang, W. P. Chan, P. Carreno-Medrano, A. Cosgun, and E. Croft, “Metrics for evaluating social conformity of crowd navigation algorithms,” in *2022 IEEE International Conference on Advanced Robotics and Its Social Impacts (ARSO)*. IEEE, 2022, pp. 1–6. 5

[54] J. L. Giesbrecht *et al.*, “A vision-based robotic follower vehicle,” in *Unmanned Systems Technology XI*, vol. 7332. SPIE, 2009, pp. 451–462. 5

[55] M. Herman *et al.*, “Pedestrian behavior prediction for automated driving: Requirements, metrics, and relevant features,” *IEEE Transactions on Intelligent Transportation Systems*, vol. 23, no. 9, pp. 14 922–14 937, 2021. 5

[56] S. H. Kiss *et al.*, “Probabilistic dynamic crowd prediction for social navigation,” in *2021 IEEE International Conference on Robotics and Automation (ICRA)*. IEEE, 2021, pp. 9269–9275. 5

## APPENDIX

### A. Localization with Long-term Anchors

In order to avoid navigation failure by the localization errors, we placed some AR tags along the topological graph to assist localization. Our idea is simply overriding the estimated node number by the node number associated with the AR tags. When collecting the topological graph, we also save the list of  $\{n_i^{ar}, p_i^{ar}, n_i^{node}\}_{i=1 \dots N_{ar}}$ . Here  $n_i^{ar}$  and  $p_i^{ar}$  are the detected AR tag number and its pose on the robot coordinate, respectively [50].  $n_i^{node}$  is the node number on the topological graph, which detects the AR tag of  $n_i^{ar}$ .

We basically override the estimated node number by  $n_j^{node}$  when detecting AR tag of  $n_i^{ar}$  in the data collection. If the multiple node images detect the same AR tag in the topological graph, we use the closest one to assist moving forward. However, the mobile robot may pass over the node location linked to the AR tag and still detect its AR tag. Such a case causes unnatural movement like stopping abruptly because the subgoal image will be behind the current robot pose. To avoid unnatural behavior, the robot compares the estimated pose of AR tag with  $p_i^{ar}$  to detect whether the its is passing by the tag. If the robot is passing by, it is overwritten with the next node number  $n_i^{ar} + 1$ .

### B. Trajectory Chaining for Continual Learning

To chain the different sequences in training, we need to take  $T_{gt}$  between current and subgoal image from different sequences. Fig. 10 visualizes how to obtain  $T_{gt}$  from different sequences. Since we place AR tags along the topological graph to assist the localization module, some frames in our dataset detect AR tag and estimate the relative pose for each AR tag. In Fig. 10,  $T_{mc}$  and  $T_{mg}$  indicate the estimated relative pose against same AR tag from different sequence  $s_c$  and  $s_g$ . Here,  $n_c$  and  $n_g$  are corresponding node number on  $s_c$  and  $s_g$ .

To take various pairs of current and subgoal images, we randomly select two step numbers within  $N_m = 18$  as  $n_{cr}$  and  $n_{gr}$  and decide the node number of the current image as  $n_c - n_{cr}$  on  $s_c$  and the node number of the subgoal image as  $n_g + n_{gr}$  on  $s_g$ , respectively. The sign of  $n_{cr}$  and  $n_{gr}$  are decided so that the subgoal image position is forward with respect to the current image position. Note that we assume that the dataset can be collected with a positive linear velocity. Since  $N_m$  is not large number, we can have accurate relative pose  $T_{oc}$  between  $n_c - n_{cr}$  and  $n_c$ , and an accurate relative pose  $T_{og}$  between  $n_g$  and  $n_g + n_{gr}$  from the odometry. As the result, we calculate  $T_{gt}$  between  $n_c - n_{cr}$  and  $n_g + n_{gr}$  as  $T_{gt} = T_{oc} \cdot T_{mc} \cdot T_{mg}^{-1} \cdot T_{og}$ .

### C. Network structures

Figure 11 describes the neural network architecture of  $\pi_\theta$ . An 8-layer CNN is used to extract the image features  $z$  from the image history  $I_{t:t-N_p}$  and the subgoal image  $I_g$ , with each layer using BatchNorm and ReLU activations. Following our previous work, ExAug, the predicted velocity commands  $\{v_i, \omega_i\}_{i=1 \dots N_s}$  from 3 fully-connected layers “FCv” are conditioned on the robot size  $\{r_s, v_l\}$  and  $z$ . A

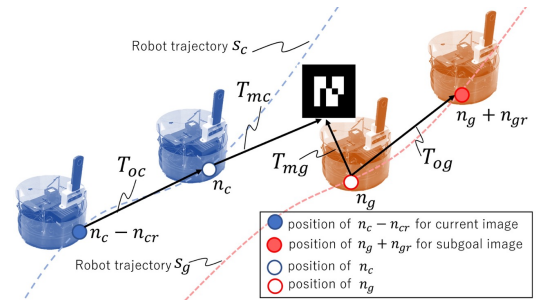


Fig. 10: **Relative positions from different sequences using AR tags.** We obtain the relative pose using the odometry of the robot and the detected pose of the AR tag for continual learning.

scaled tanh activation is given to limit the output velocities as per the specified constraints. We can control the robot by giving  $v_1$  and  $\omega_1$  as the actual robot velocity command.

In addition to the core part of our control policy, we can implement “FCt” to estimate traversability  $\{t_i\}_{i=1 \dots N_s}$ , following ExAug. We integrate the velocities to obtain waypoints predictions and feed them to a set of fully-connected layers “FCt” along with the observation embedding  $z$  and target robot size  $r_s'$ , followed by a sigmoid function to limit  $t_i \in (0, 1)$ . Although  $r_s = r_s'$  in training, we found the flexibility of an independent  $r_s' \neq r_s$  crucial to the collision-avoidance performance of our system in inference. Note that we can remove the gray color part to construct  $\pi_\theta$  for the minimum implementation.

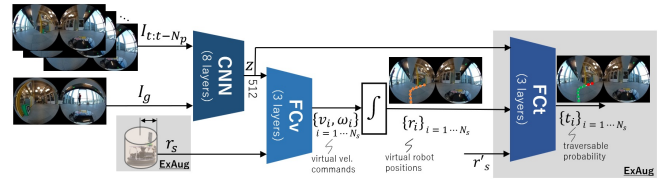


Fig. 11: **Network structure of our control policy.**

In our evaluation section, we train the predictive model  $f_{\theta_p}$  for the pedestrians dynamics. Fig. 12 is the network structure of  $f_{\theta_p}$ . At first, we feed the concatenated past human trajectory  $h_{t-\alpha:t-1}$  and the past robot trajectory  $r_{t-\alpha:t-1}$  into “FC1” with the three fully connected layers using BatchNorm and ReLU activations to extract the features  $z_p$ . Then, we predict the human future trajectory condition on the robot actions (=future trajectories) by giving  $z_p$  with  $r_{t-1:t+\beta}$ . Here, the last layer of “FC2” with three fully connected layers has the tanh activation to limit the human velocity within  $\pm 1.5$  m/s.

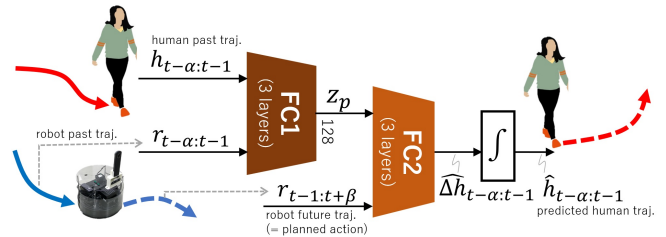


Fig. 12: **Network structure of our model to predict pedestrians dynamics.**